



OPEN ACCESS

EDITED BY

Jesus Manuel Munoz-Pacheco,
Benemérita Universidad Autónoma de
Puebla, Mexico

REVIEWED BY

Kehui Sun,
Central South University, China
Aceng Sambas,
Muhammadiyah University of
Tasikmalaya, Indonesia

*CORRESPONDENCE

Chunhua Wang,
✉ wch1227164@hnu.edu.cn

RECEIVED 07 August 2023

ACCEPTED 23 August 2023

PUBLISHED 08 September 2023

CITATION

Hu Z, Lin H and Wang C (2023), A novel
grid multi-structure chaotic attractor and
its application in medical
image encryption.

Front. Phys. 11:1273872.

doi: 10.3389/fphy.2023.1273872

COPYRIGHT

© 2023 Hu, Lin and Wang. This is an
open-access article distributed under the
terms of the [Creative Commons
Attribution License \(CC BY\)](#). The use,
distribution or reproduction in other
forums is permitted, provided the original
author(s) and the copyright owner(s) are
credited and that the original publication
in this journal is cited, in accordance with
accepted academic practice. No use,
distribution or reproduction is permitted
which does not comply with these terms.

A novel grid multi-structure chaotic attractor and its application in medical image encryption

Zhenhua Hu^{1,2}, Hairong Lin¹ and Chunhua Wang^{1*}

¹College of Computer Science and Electronic Engineering, Hunan University, Changsha, China, ²College of Science, Hunan City University, Yiyang, China

Grid multi-scroll/wing chaotic systems are complex non-linear dynamic systems, which are widely used in secure communication. The grid multi-scroll/wing chaotic systems are usually realized by using the function control method, which has a complex realization method, many control parameters, and a simple unit attractor structure. In this paper, based on the Hopfield neural network, a memristive Hopfield neural network model is proposed by using the memristor synapse control method. The model can generate novel grid multi-structure chaotic attractors, which have the characteristics of a simple implementation method, few control parameters, and complex unit attractor structure. Firstly, the generation mechanism of the grid multi-structure chaotic attractors is analyzed by the equilibrium points and stability. Secondly, its basic dynamical characteristics including the Lyapunov exponent spectrum, fractal dimension, time series, power spectrum, bifurcation diagram, and Poincaré section are analyzed. Thirdly, an analog circuit of the neural network model is designed and realized by Multisim. Finally, combined with the chaos encryption principle, an image encryption scheme is designed based on the generated grid multi-structure attractors. Experimental results show that compared with the existing schemes, the proposed scheme has larger information entropy, higher key sensitivity, and a good application prospect.

KEYWORDS

multi-structure attractor, memristor, Hopfield neural network, image encryption, circuit implementation

1 Introduction

Chaos theory is an important discovery of human natural science in the 20th century and has been widely concerned in the fields of non-linear circuits, neural networks, information security, and so on [1–3]. Chaotic attractors are the core of chaos theory, which corresponds to the motion of a disordered steady state in a chaotic system. Since Lorenz [4] discovered the first double-wing attractor in 1962, the construction of complex attractors in chaotic systems has been an important topic in the field of chaos research. After years of exploration, many chaotic systems with different types of attractors have been discovered [5–8], but a complete theoretical model has not yet been developed. The study of chaotic attractors is a very important and key link in the study of chaos theory. From the whole research process, the study of chaotic attractors has just started, and more chaotic attractors are still to be explored and discovered. Furthermore, the wide application of chaotic signals generated by chaotic

attractors in the field of information security is another reason that attracts many researchers.

At present, there are three types of chaotic attractors found at home and abroad: 1) Self-excited attractors and hidden attractors. The chaotic attractors discovered earlier are closely related to the unstable equilibrium point of the system and are called self-excited attractors, such as the classical Lorenz attractors [4], Chua's attractors [9], Chen attractors [10], Lv attractors [11] and so on [12–16]. With the deepening of research on self-excited attractors, some scholars have found that there is an attractor basin of chaos that does not intersect with any open small neighborhood of the equilibrium point of the system, which is called a hidden attractor [17]. In recent years, various hidden attractors have been proposed, such as the hidden attractor of no equilibrium point [18], the hidden attractor of a stable equilibrium point [19], and the hidden attractor of infinite equilibrium points [20]. 2) transient chaotic attractors, chaotic attractors, and hyperchaotic attractors. Chaotic systems can be characterized by the Lyapunov exponent, and chaotic attractors can be divided into different types according to the maximum Lyapunov exponent spectrum. In general, a transient chaotic attractor is defined as the existence of a positive Lyapunov exponent in finite time [21]. The attractor has a positive Lyapunov exponent in infinite time and is called a chaotic attractor. Hyperchaotic attractors are defined as the simultaneous existence of two or more positive Lyapunov exponents in infinite time [22]. In the past few decades, the research on transient chaotic attractors, chaotic attractors, and hyperchaotic attractors has been fruitful [23–25]. 3) Double scroll/wing attractor, multi-scroll/wing attractor, and grid multi-scroll/wing attractor. Double scroll/wing attractors are classical chaotic attractors with special scroll and dynamic trajectories of butterfly wings. Many simple chaotic systems can produce double scroll/wing attractors, such as Chua's system, Lorenz system, Sprott system [26], Jerk circuit [27], and so on [28, 29]. With the deepening of research on double scroll/wing attractors, various functions such as periodic function [30], piecewise linear function [31], and multistage logic pulse function [32] have been used to expand double scroll/wing attractors in multiple directions to generate multi-scroll/wing attractors [33–35] and grid multi-scroll/wing attractors [36–38]. Among them, the grid multi-scroll/wing attractor has flexible adjustability and high complexity and has a very broad application prospect in secure communication and chaos control [39, 40], so it has become a research hotspot in academia.

The artificial neural network is a kind of non-linear system with complex dynamic characteristics [41, 42]. In recent years, the study of neural network dynamics has gradually become a new research hotspot in the intersection of physics, mathematics, computer science, and neuroscience [43–45]. Among them, Hopfield neural network is a complex non-linear system with chaotic behaviors [46]. Due to its chaotic characteristic, various Hopfield neural network models with different neurons and synaptic weights have been proposed and analyzed [47–50]. In particular, memristive Hopfield neural networks have attracted much attention because of their complex chaotic behavior and potential applications in image encryption. For example, Lin et al. [51] constructed a memristive Hopfield neural network with an arbitrary number of scroll attractors. Yu et al. [52, 53] designed two different memristive Hopfield neural networks which can generate multi-double-scroll

attractors. Furthermore, Lai et al. [54] proposed a memristive Hopfield neural network with grid multi-scroll attractors. Meanwhile, the memristive neural network is used to design an image encryption scheme. Although the grid multi-scroll/wing attractor has excellent characteristics, the existing grid multi-scroll/wing attractor implementation methods are complex, the unit structure is simple, and the control parameters are many, and the exploration in recent years seems to indicate that the research of grid multi-scroll/wing attractor is difficult to make updated progress.

To solve these problems, this paper proposes a new method for the generation of novel grid multi-structure chaotic attractors controlled by memristor synapses based on the Hopfield neural network. This method is based on the neural network with complex dynamic characteristics, which successfully gets rid of the scroll/wing attractor unit structure, and makes it appear a more complex and changeable chaotic attractor unit structure. In addition, only two memristor synaptic control parameters are needed to adjust the grid size of the chaotic attractor. The basic dynamic characteristics of the new grid multi-structure attractor are studied by theoretical analysis and numerical simulation. At the same time, the existence of the attractor is verified from the aspect of the circuit. Finally, a scheme of grid multi-structure attractor image encryption is designed based on chaotic encryption theory. The experimental results show that the chaotic attractor exhibits complex dynamic characteristics, so it has better encryption performance and effect in image encryption.

The rest of this paper is organized as follows. Section 2 constructs a memristive Hopfield neural network. Section 3 analyzes the dynamical behaviors of the neural network. Section 4 designs and implements an analog neural network circuit. Section 5 designs a medical image encryption scheme. Section 6 concludes the article.

2 Construction of grid multi-structure attractors

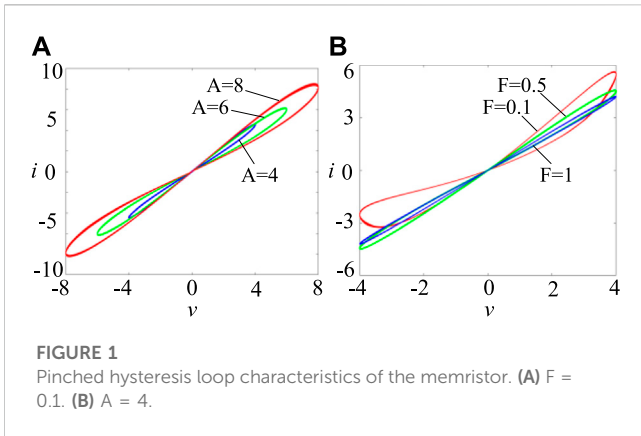
2.1 Introduction of memristor and Hopfield neural network

A memristor is a non-linear circuit element with synaptic memory properties [55], often described in terms of voltage and current relationships. In this paper, a multi-piecewise non-linear flux-controlled memristor model is introduced [51], which can be expressed as

$$\begin{cases} i = (a + b\varphi)v \\ \dot{\varphi} = cv - dh(\varphi) \end{cases} \quad (1)$$

where a , b , c , and d represent the four positive parameters of the memristor, and $W(\varphi) = (a + b\varphi)$ represents the memristor conductance associated with the memristor state variable φ . In addition, $h(\varphi)$ is the internal state variable function of the memristor, which can be expressed as

$$h(\varphi) = \begin{cases} h_1(\varphi) \\ h_2(\varphi) \end{cases} \quad (2)$$



where

$$h_1(\varphi) = \begin{cases} \varphi, N = 0 \\ \varphi - \sum_{i=1}^N (\text{sgn}(\varphi + (2i - 1)) + \text{sgn}(\varphi - (2i - 1))) \\ N = 1, 2, 3, \dots \end{cases} \quad (3)$$

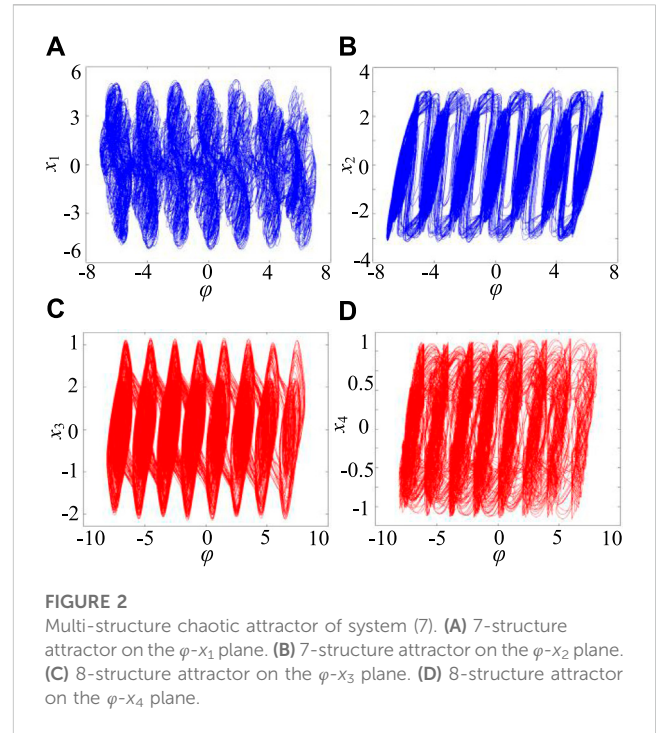
$$h_2(\varphi) = \begin{cases} \varphi - \text{sgn}(\varphi), M = 0 \\ \varphi - \text{sgn}(\varphi) - \sum_{j=1}^M (\text{sgn}(\varphi + 2j) + \text{sgn}(\varphi - 2j)) \\ M = 1, 2, 3, \dots \end{cases} \quad (4)$$

the $\text{sgn}(\cdot)$ is a symbolic function, N and where M are the two control parameters of the memristor. To verify that the above mathematical model is a memristor model, consider the case when $N = 3$. With fixed memristor parameters $a = 1, b = 0.05, c = 2.2, d = 1.2, \varphi_0 = 0$, the pinched hysteresis loop of the memristor is simulated by MATLAB R2017a when sinusoidal voltage $v = A\sin(2\pi Ft)$ is applied at both ends of the memristor. The simulation results are shown in Figure 1. Under different excitation amplitude A , the pinched hysteresis loop of the model always passes through the origin of the voltage and current plane. With the increase of voltage frequency F , the area of the pinched hysteresis loop of the memristor decreases gradually. When the voltage frequency increases to infinity, the pinched hysteresis loop shrinks to a one-valued function. In summary, the proposed mathematical model satisfies the three characteristics of the memristor and is a memristor model.

The Hopfield neural network can produce complex chaotic phenomena and is a classical model for studying chaotic dynamics. A Hopfield neural network with n neurons can be expressed as [46]

$$C_i \dot{v}_i = -\frac{v_i}{R_i} + \sum_{j=1}^n w_{ij} \tanh(v_j) + I_i (i, j \in N^*) \quad (5)$$

where, C_i, v_i and R_i respectively represent the membrane capacitance, membrane voltage and membrane resistance of neuron i . w_{ij} represents the synaptic connection weight from neuron j to neuron i , and $\tanh(\cdot)$ is the neuronal activation function. In addition, I_i represents the external bias current of the neuron. Generally speaking, the dynamic behavior of the Hopfield neural network is closely related to its synaptic weight coefficient. According to neural network model (Eq. 5), a Hopfield neural network model with four neurons is constructed by selecting



appropriate synaptic weight coefficients, let $C_i = 1, R_i = 1, I_i = 0$, and its expression is as follows

$$\begin{cases} \dot{x}_1 = -x_1 + 3\tanh(x_2) + 3\tanh(x_3) - 13\tanh(x_4) \\ \dot{x}_2 = -x_2 - \tanh(x_1) + 1.5\tanh(x_2) + 7\tanh(x_3) - 5\tanh(x_4) \\ \dot{x}_3 = -x_3 - 4\tanh(x_2) + 1.8\tanh(x_3) + 4\tanh(x_4) \\ \dot{x}_4 = -x_4 + 0.7\tanh(x_1) + 2\tanh(x_4) \end{cases} \quad (6)$$

where $x_i (i = 1, 2, 3, 4)$ is the membrane voltage of neuron i .

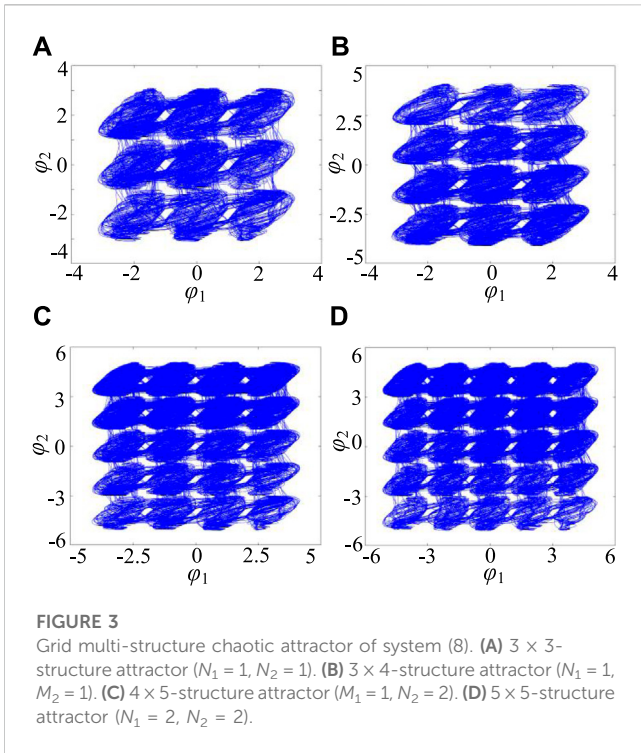
2.2 Construction of single-directional multi-structure attractors

Memristors have synaptic memory and programmability and can be used to simulate neural synapses [55]. When replacing the resistive synapses between neuron 3 and neuron 1 in the neural network (6) with the multi-piecewise non-linear memristor (1) described above, a memristive Hopfield neural network can be constructed as follows

$$\begin{cases} \dot{x}_1 = -x_1 + 3\tanh(x_2) + \rho W(\varphi)\tanh(x_3) - 13\tanh(x_4) \\ \dot{x}_2 = -x_2 - \tanh(x_1) + 1.5\tanh(x_2) + 7\tanh(x_3) - 5\tanh(x_4) \\ \dot{x}_3 = -x_3 - 4\tanh(x_2) + 1.8\tanh(x_3) + 4\tanh(x_4) \\ \dot{x}_4 = -x_4 + 0.7\tanh(x_1) + 2\tanh(x_4) \\ \dot{\varphi} = c \tanh(x_3) - d h(\varphi) \end{cases} \quad (7)$$

where, ρ represents the memristor synaptic coupling strength, $\rho W(\varphi) = \rho(a + b\varphi)$ represents the memristor synaptic coupling weight.

When $a = 1, b = 0.01, c = 2.2, d = 1.2, \rho = 3$, the initial value (0.1, 0.1, 0.1, 0.1, 0.1), the system in the φ -axis can produce n structure attractor. Taking $N = 3$ and $M = 3$ respectively, the numerical



simulation results of 7-structure chaotic attractor and 8-structure chaotic attractor are obtained according to the system (7), as shown in Figure 2. From the attractor substructure in Figure 2, it is not difficult to find that, unlike the multi-scroll/wing chaotic attractor, the multi-structure chaotic attractor contains the unit structure attractor with multiple trajectory-disorder, rather than the conventional scroll/wing.

2.3 Construction of grid multi-structure attractors

Further studies show that the chaotic attractor can be reconstructed and expanded in different directions by using other synapses in the same type of multi-segment non-linear memristor synaptic replacement system (7), and the grid multi-structure chaotic attractor can be constructed. The system model is as follows

$$\begin{cases} \dot{x}_1 = -x_1 + 3 \tanh(x_2) + \rho_1 W(\varphi_1) \tanh(x_3) - 13 \tanh(x_4) \\ \dot{x}_2 = -x_2 - \tanh(x_1) + 1.5 \tanh(x_2) + 7 \tanh(x_3) - \rho_2 W(\varphi_2) \tanh(x_4) \\ \dot{x}_3 = -x_3 - 4 \tanh(x_2) + 1.8 \tanh(x_3) + 4 \tanh(x_4) \\ \dot{x}_4 = -x_4 + 0.7 \tanh(x_1) + 2 \tanh(x_4) \\ \dot{\varphi}_1 = c \tanh(x_3) - dh(\varphi_1) \\ \dot{\varphi}_2 = c \tanh(x_4) - dh(\varphi_2) \end{cases} \quad (8)$$

where ρ_i represents the memristor synaptic coupling strength, $\rho_i W(\varphi_i) = \rho_i(a + b\varphi_i)$ represents the memristor synaptic coupling weight.

Select $a = 1, b = 0.01, c = 2.2, d = 1.2, \rho_1 = 3, \rho_2 = 5$, and the initial value is $(0.1, 0.1, 0.1, 0.1, 0.1)$. By taking different memristor control parameters N_i and M_i , the $n \times m$ grid multi-structure chaotic attractor can be obtained from system (8), as shown in Figure 3.

TABLE 1 Relation between memristor synaptic control parameters and grid attractors.

N_i/M_i	$\varphi_1 (n)$	N_2/M_2	$\varphi_2 (m)$
0	1/2	0	1/2
1	3/4	1	3/4
2	5/6	2	5/6
...
N/M	$(2N + 1)/(2M + 2)$	N/M	$(2N + 1)/(2M + 2)$

Obviously, by controlling the two control parameters of the two memristor synapses, a grid multi-structure chaotic attractor of arbitrary size can be obtained, as shown in Table 1. Therefore, compared with the existing multi-parameter function control methods of grid multi-scroll/wing chaotic attractors [30–32], the proposed control method of grid multi-structure chaotic attractors is greatly simplified. In addition, by comparing the structure of system (7) and system (8), we can see that: Only one memristor synapse is introduced in system (7), so that the attractor expands horizontally in the direction of introducing the magnetic flux variable φ , while system (8) introduces two memristor synapses at the same time, so that the attractor expands simultaneously in both directions of the magnetic flux variable φ_1 and the magnetic flux variable φ_2 , thus forming a more complex grid multi-structure chaotic attractor. This is a phenomenon that has not been seen in many chaotic structures before.

3 Basic dynamics analysis

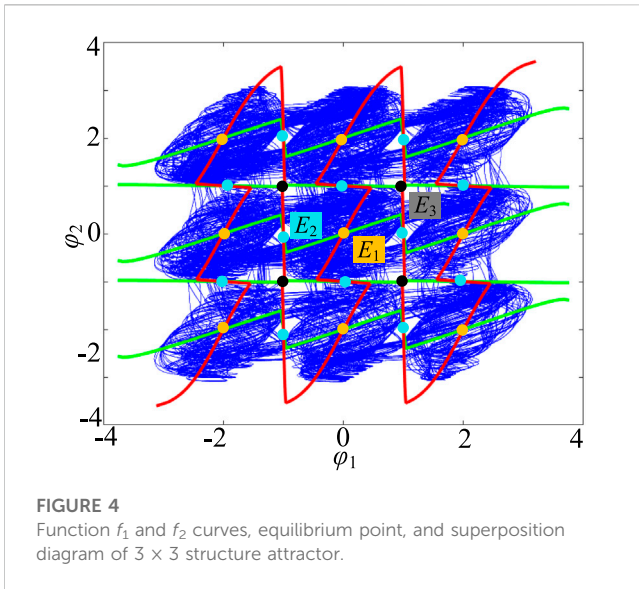
In this section, the dynamic generation mechanism and chaotic characteristics of system (8) are analyzed by dynamic analysis method and numerical simulation.

3.1 Equilibrium points and their stabilities

The equilibrium point is a necessary condition for the generation of self-excited chaos, which can reveal the formation mechanism of chaos attractor from the system level. If the right-hand side of Eq. 8 is equal to 0, the equilibrium state equation of the system can be obtained as follows

$$\begin{cases} -x_1 + 3 \tanh(x_2) + \rho_1 W(\varphi_1) \tanh(x_3) - 13 \tanh(x_4) = 0 \\ -x_2 - \tanh(x_1) + 1.5 \tanh(x_2) + 7 \tanh(x_3) - \rho_2 W(\varphi_2) \tanh(x_4) = 0 \\ -x_3 - 4 \tanh(x_2) + 1.8 \tanh(x_3) + 4 \tanh(x_4) = 0 \\ -x_4 + 0.7 \tanh(x_1) + 2 \tanh(x_4) = 0 \\ c \tanh(x_3) - dh(\varphi_1) = 0 \\ c \tanh(x_4) - dh(\varphi_2) = 0 \end{cases} \quad (9)$$

Equation 9 is a sixth-order equation, using the MATLAB platform to solve the equilibrium point by graphical analysis method. To have resistance control parameters $N_1 = N_2 = 1$ as an example, set $a = 1, b = 0.01, c = 2.2, d = 1.2, \rho_1 = 3, \rho_2 = 5$, Eq. 9 can be converted to

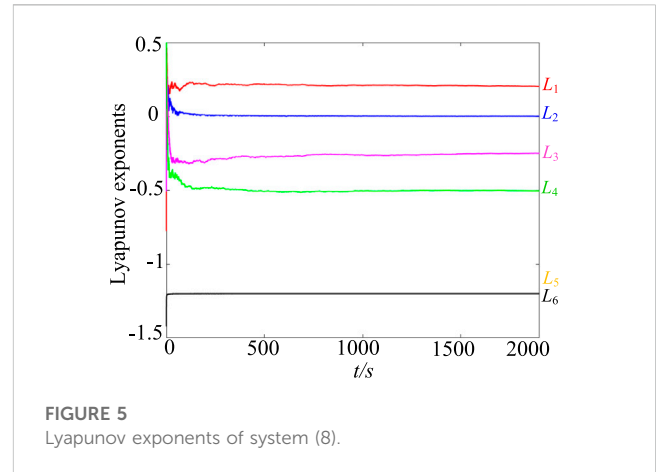


$$\begin{cases} x_3 = \operatorname{atanh}(dh(\varphi_1)/c) \\ x_4 = \operatorname{atanh}(dh(\varphi_2)/c) \\ x_1 = \operatorname{atanh}((x_4 - 2\tanh(x_4))/0.7) \\ x_2 = \operatorname{atanh}((-x_3 + 1.8\tanh(x_3) + 4\tanh(x_4))/4) \\ f_1(\varphi_1, \varphi_2) = -x_1 + 3\tanh(x_2) + \rho_1 W(\varphi_1)\tanh(x_3) - 13\tanh(x_4) = 0 \\ f_2(\varphi_1, \varphi_2) = -x_2 - \tanh(x_1) + 1.5\tanh(x_2) + 7\tanh(x_3) - \rho_2 W(\varphi_2)\tanh(x_4) = 0 \end{cases} \quad (10)$$

The functions f_1 and f_2 are drawn in MATLAB R2017a, as shown in Figure 4, where f_1 is represented by a green curve and f_2 by a red curve. It can be observed from the figure that f_1 and f_2 have 25 intersection points in different positions, that is, the system (8) has 25 equilibrium points at this time. Near the equilibrium point, the Jacobian matrix of the system can be expressed as

$$J = \begin{bmatrix} -1 & 3m_2 & \rho_1 W(\varphi_1)m_3 & -13m_4 & \rho_1 b \tanh(x_3) & 0 \\ -m_1 & -1 + 1.5m_2 & 7m_3 & -\rho_2 W(\varphi_2)m_4 & 0 & -\rho_2 b \tanh(x_4) \\ 0 & -4m_2 & -1 + 1.8m_3 & 4m_4 & 0 & 0 \\ 0.7m_1 & 0 & 0 & -1 + 2m_4 & 0 & 0 \\ 0 & 0 & cm_3 & 0 & -dh'(\varphi_1) & 0 \\ 0 & 0 & 0 & cm_4 & 0 & -dh'(\varphi_2) \end{bmatrix} \quad (11)$$

where $m_i = \operatorname{sech}^2(x_i)$, $i = 1, 2, 3, 4$. Through numerical calculation, these 25 equilibrium points have three different stability, namely, unstable saddle coke of indicator 4 (yellow), unstable saddle coke of indicator 5 (blue), and unstable saddle coke of indicator 6 (black), as shown in Table 2. Obviously, system (8) generates 9 single structure attractors in the neighborhood of 9 unstable saddle focal points with index-4, 10 unstable saddle focal points with index-5 produce bond bands in the direction of φ_1 and φ_2 , and 4 unstable saddle focal points with index-6 play a role in strengthening the connection in the diagonal direction. Finally, under the action of 25 unstable



equilibrium points, a 3×3 grid multi-structure chaotic attractor phenomenon is generated, as shown in Figure 4. A large number of simulation results show that with the increase of the control parameters N_1/M_1 and N_2/M_2 of the two memristic synapses, the equilibrium point of the system will gradually expand along the φ_1 and φ_2 axes, resulting in a larger number of grid multi-structure chaotic attractors on the φ_1 - φ_2 phase plane.

3.2 Lyapunov exponents and Kaplan-Yorke dimension

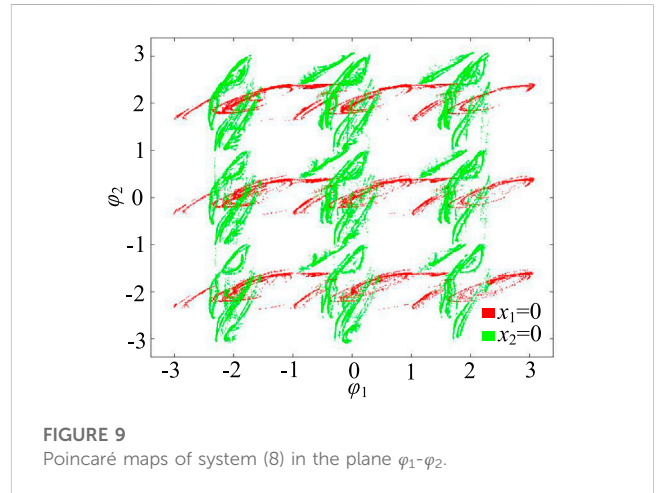
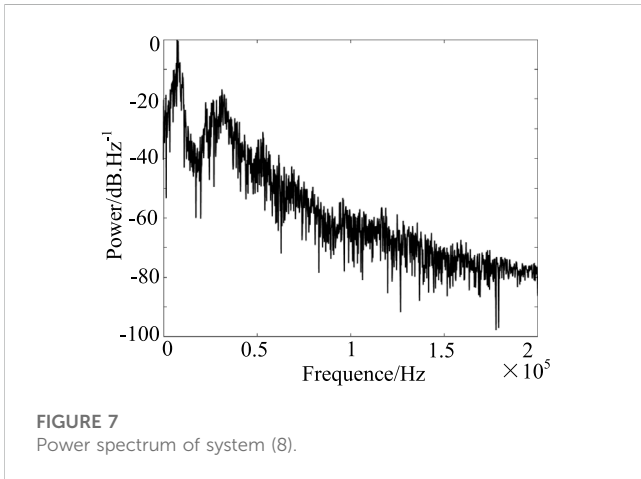
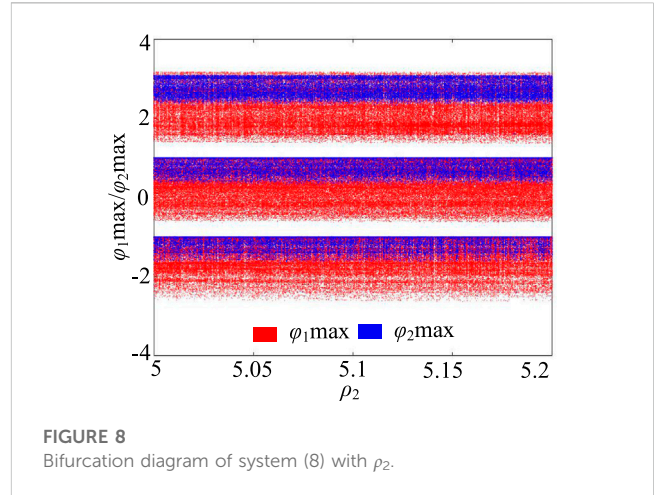
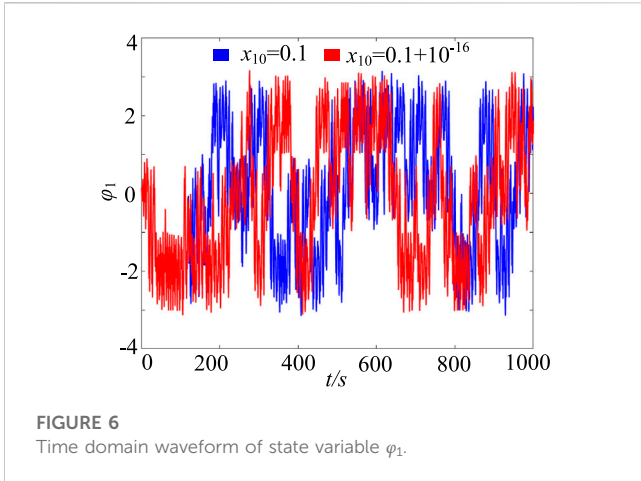
Lyapunov exponent spectrum analysis is an important method to study the dynamical characteristics of chaotic systems. It reveals the chaotic characteristics of the system from the perspective of the average exponential rate of convergence or divergence between adjacent orbits in the phase space of the system. Under the condition of multi-structure attractor generation in a 3×3 grid, six Lyapunov indices of the system were obtained by using the Wolf's Jacobian-based method, as shown in Figure 5. Where $L_1 = 0.2146$, $L_2 = 0.0015$, $L_3 = -0.2608$, $L_4 = -0.5047$, $L_5 = -1.201$, $L_6 = -1.202$. Obviously, it is not difficult to find that system (8) has a positive Lyapunov exponent; a Lyapunov exponent is approaching 0; The sum of all Lyapunov exponents is negative. Therefore, under these conditions, the system is chaotic. The Kaplan-Yorke dimension corresponding to its Lyapunov index is

$$D_{KY} = j + \frac{1}{|L_{j+1}|} \sum_{i=1}^j L_i = 2 + \frac{L_1 + L_2}{|L_3|} = 2.8286 \quad (12)$$

Obviously, the Kaplan-Yorke dimension of the system is fractional, which further proves that the grid multi-structure attractors generated by the system are chaotic.

TABLE 2 Representative equilibrium points of system (8), corresponding to eigenvalues and types of equilibrium points.

Equilibrium points	Eigenvalues	Stabilities
$E_1 (0,0,0,0,0)$	$(-1.2, -1.2, 0.3181 \pm 5.9165i, 0.3319 \pm 1.9652i)$	unstable saddle focus with index 4
$E_2 (0,0,0,0,-1,0)$	$(1.2e + 6, -1.2, 0.3213 \pm 5.9156i, 0.3286 \pm 1.9678i)$	unstable saddle focus with index 5
$E_3 (0,0,0,0,1,1)$	$(1.2e + 6, 1.2e + 6, 0.3165 \pm 5.9186i, 0.3335 \pm 1.9586i)$	unstable saddle focus with index 6



3.3 Time series and power spectrum

When system parameters are kept unchanged, the timing waveform of system (8) in the direction of state variable φ_1 is shown by the blue curve in Figure 6. It can be seen from the figure that its motion trajectory oscillates randomly in a certain region and has distinct aperiodic characteristics. In addition, after slightly changing the initial value x_{10} , the time-domain waveform obtained by system (8) is shown by the red curve in Figure 6. It is not difficult to see that when the initial values are 0.1 and $0.1 + 10^{-16}$ respectively, there is no obvious difference between the two timings in (0, 120 s) time, but when t is greater than 120 s, they show completely different time evolution tracks. Therefore, even with a size adjustment of 10^{-16} for x_{10} , the trajectory of the system can make a huge difference, which means that the motion state of the system is not only aperiodic but also extremely sensitive to initial conditions. To further verify its non-periodicity, the power spectrum of system (8) is shown in Figure 7. It can be seen that the system exhibits a continuous power spectrum similar to a noise signal in a limited frequency range, which indicates that the system has obvious aperiodic chaotic characteristics.

3.4 Bifurcation diagrams and Poincaré maps

The bifurcation diagram is an important tool to describe the dynamic state of chaotic systems with parameter variation. Figure 8 shows the structure of local branch forks within the range of parameter $\rho_2 \in [5, 5.2]$, where red is the bifurcation in the direction of state variable φ_1 , and blue is the bifurcation in the direction of state variable φ_2 . It can be seen from Figure 8 that there are pieces of quasi-random points in the bifurcation diagram, indicating that the system is in a chaotic state. More importantly, different from the general chaotic bifurcation structure, the bifurcation diagram of system (8) presents three parallel bifurcation structures simultaneously in the directions of φ_1 and φ_2 , and they are all in a chaotic state. This means that the system generates a 3×3 grid multi-structure chaotic attractor. In addition, Figure 9 shows the Poincaré map of a 3×3 grid multi-structure chaotic attractor in the φ_1 - φ_2 phase plane. Among them, the red section diagram is generated by the $x_1 = 0$ section, and the green section diagram is generated by the $x_2 = 0$ section. Through observation, it is not difficult to find that the Poincaré map of system (8) shows a series of irregular dense points, which further

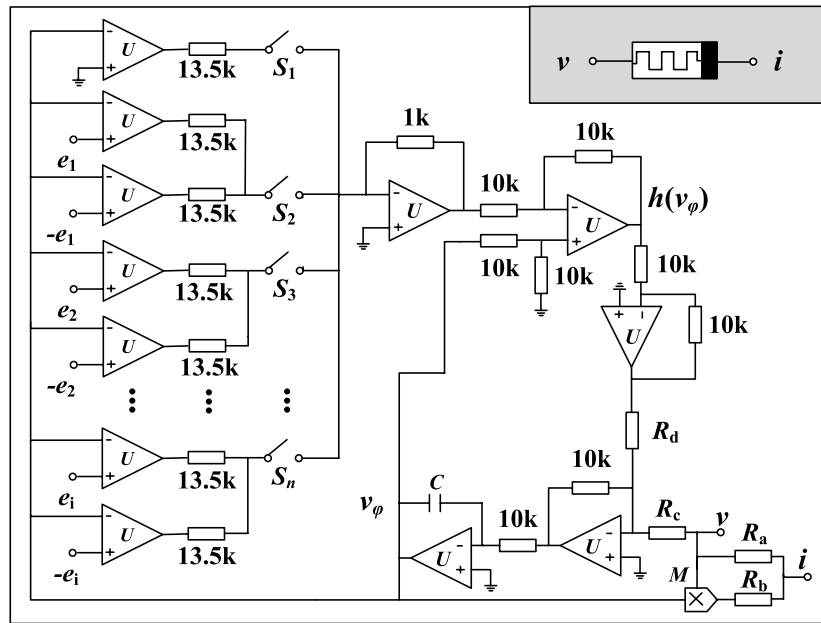


FIGURE 10 Memristor circuit.

proves that the grid multi-structure attractors have complex chaotic characteristics.

4 Circuit implementation and verification

Circuit realization is one of the effective ways to verify the mathematical model [56]. In general, chaotic systems can be implemented by analog or digital circuits to generate chaotic signals [57, 58]. In this section, we first design the physical circuit of system (8) and then verify the existence of grid multi-structure chaotic attractors by Multisim simulation.

4.1 Circuit design

First, a multi-segment non-linear memristor circuit is designed, as shown in Figure 10. Where, the internal state equation $h(\varphi)$ of the memristor is realized by a non-linear function generator, e_1, e_2, \dots, e_i is the control voltage, S_1, S_2, \dots, S_n is the selection switch. By selecting the corresponding control voltage and switch, the memristor function under different control parameters can be realized, as shown in Table 3.

Then, based on the memristor circuit, the physical circuit of system (8) is realized, as shown in Figure 11. Where the neuron activation function $\tanh(\cdot)$. The equivalent circuit is available in Ref. [47]. In addition, the four neuronal membrane voltages are simulated by the four capacitor voltages of the circuit, and the fixed synaptic weight coefficients are simulated using resistors R_1-R_{10} . The memristor synaptic weight is achieved by the memristor. According to Kirchhoff's current law, the circuit equation of system (8) can be expressed as

$$\begin{cases} RC\dot{v}_1 = -v_1 + \frac{R}{R_1} \tanh(v_2) + R \left(\frac{1}{R_{a1}} + g \frac{v_{\varphi 1}}{R_{b1}} \right) \tanh(v_3) - \frac{R}{R_2} \tanh(v_4) \\ RC\dot{v}_2 = -v_2 - \frac{R}{R_3} \tanh(v_1) + \frac{R}{R_4} \tanh(v_2) + \frac{R}{R_5} \tanh(v_3) - R \left(\frac{1}{R_{a2}} + g \frac{v_{\varphi 2}}{R_{b2}} \right) \tanh(v_4) \\ RC\dot{v}_3 = -v_3 - \frac{R}{R_7} \tanh(v_2) + \frac{R}{R_8} \tanh(v_3) + \frac{R}{R_9} \tanh(v_4) \\ RC\dot{v}_4 = -v_4 + \frac{R}{R_{10}} \tanh(v_1) + \frac{R}{R_{11}} \tanh(v_4) \\ RC\dot{v}_{\varphi 1} = \frac{R}{R_c} \tanh(v_3) - \frac{R}{R_d} h(v_{\varphi 1}) \\ RC\dot{v}_{\varphi 2} = \frac{R}{R_c} \tanh(v_3) - \frac{R}{R_d} h(v_{\varphi 2}) \end{cases} \quad (13)$$

4.2 MULTISIM simulation

The physical circuit of system (8) is implemented and simulated on the Multisim14.0 platform. In this section, we first design the physical circuit of system (8) and then verify the existence of grid multi-structure chaotic attractors by Multisim simulation. Set capacitance $C = 1 \text{ nF}$, $R = 10 \text{ k}\Omega$. Fixed synaptic weight coefficient according to system (8), setting $R_1 = R/w_{12} = 3.3 \text{ k}\Omega$, $R_2 = R/w_{14} = 0.77 \text{ k}\Omega$, $R_3 = R/w_{21} = 10 \text{ k}\Omega$, $R_4 = R/w_{22} = 6.7 \text{ k}\Omega$, $R_5 = R/w_{23} = 1.4 \text{ k}\Omega$, $R_6 = R/w_{32} = 2.5 \text{ k}\Omega$, $R_7 = R/w_{33} = 5.7 \text{ k}\Omega$, $R_8 = R/w_{34} = 2.5 \text{ k}\Omega$, $R_9 = R/w_{41} = 14.3 \text{ k}\Omega$, $R_{10} = R/w_{44} = 5 \text{ k}\Omega$. In addition, the resistance of the memristor circuit $R_a = R/pa$, $R_b = gR/pb$, $R_c = R/c$, $R_d = R/d$. When the system parameters $a = 1$, $b = 0.01$, $c = 2.2$, $d = 1.2$, $\rho_1 = 3$, $\rho_2 = 5$, $R_{a1} = 3.3 \text{ k}\Omega$, $R_{b1} = 34 \text{ k}\Omega$, $R_{a2} = 2 \text{ k}\Omega$, $R_{b2} = 20 \text{ k}\Omega$, $R_c = 4.5 \text{ k}\Omega$, $R_d = 8.4 \text{ k}\Omega$ can be solved. Set the initial voltage of the five capacitor voltages to (0.1V, 0.1V, 0.1V, 0.1V). By setting the corresponding switching and control voltage according to Table 3, the system circuit can generate a grid multi-structure chaotic attractor consistent with the numerical simulation results, as

TABLE 3 Different memristor types realized by selecting the combination of switch and control voltage.

S_1	S_2	S_3	S_4	...	S_n	Memristor
$e_1 = 1\text{ V}$	$e_2 = 3\text{ V}$	$e_3 = 5\text{ V}$	$e_4 = 7\text{ V}$...	$e_i=(2n-1)\text{ V}$	$h_1(\varphi)$
Open	Open	Open	Open	...	Open	$N = 0$
Open	Off	Open	Open	...	Open	$N = 1$
Open	Off	Off	Open	...	Open	$N = 2$
...
$e_1 = 2\text{ V}$	$e_2 = 4\text{ V}$	$e_3 = 6\text{ V}$	$e_4 = 8\text{ V}$...	$e_i=(2n)\text{ V}$	$h_2(\varphi)$
闭合	断开	断开	断开	...	断开	$M = 0$
闭合	闭合	断开	断开	...	断开	$M = 1$
闭合	闭合	闭合	断开	...	断开	$M = 2$
...

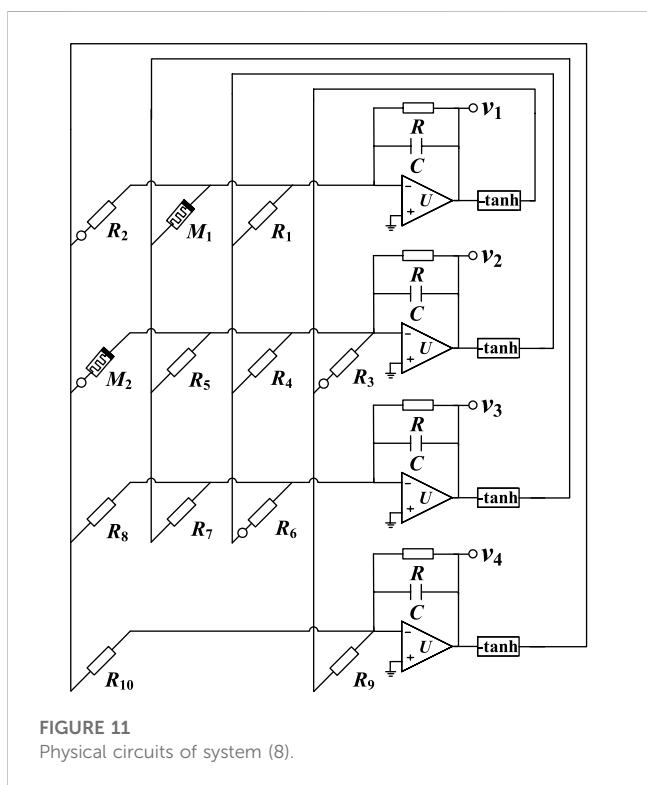


FIGURE 11 Physical circuits of system (8).

shown in Figure 12. By comparing the results of Figure 12 and Figure 13, it can be found that the results obtained by Multisim circuit simulation and Matlab numerical simulation are almost exactly the same, thus verifying the grid multi-structure chaotic attractor characteristics of system (8).

5 Medical image encryption applications

Chaotic signals have the characteristics of ergodic, initial value sensitivity, high randomness, etc., and are mainly used for the key

generation of secure communication [59, 60]. Generally, the more chaotic the attractor trajectory of chaotic systems, the more sensitive the initial conditions, the higher the randomness of the key generated, and the better the encryption performance. Based on the above analysis results, the grid multi-structure chaotic attractor proposed in this paper has a complex structure, high initial value sensitivity, and strong chaos randomness, which can greatly improve the communication encryption effect and crack difficulty.

5.1 Image encryption scheme

In this section, a new image encryption scheme is designed based on the grid multi-structure chaotic attractor. The specific encryption steps are as follows:

Step 1: Set $(a, b, c, d, \rho_1, \rho_2, x_{20}, x_{30}, x_{40}, \varphi_{10}, \varphi_{20}, N_1, N_2) = (1, 0.01, 2.2, 1.2, 3, 5, 0.1, 0.1, 0.1, 0.1, 0.1, 1, 1)$, discarded number $N_0 = 1000$, time step $\Delta t = 0.002$, based fourth-order Runge-Kutta algorithm, the system (8) is continuously iterated 256×256 times. For each iteration, we can get six values $x_1(i), x_2(i), x_3(i), x_4(i), \varphi_1(i), \varphi_2(i)$.

Step 2: The following preprocessing is performed on the six chaotic sequences to produce two distinct sets of sequences, respectively

$$K_1(i) = x_{1i} + x_{2i} + x_{3i} + x_{4i} \tag{14}$$

$$K_2(i) = \text{mod}(\text{floor}(((x_{1i} + x_{2i} + x_{3i} + x_{4i} + \varphi_{1i} + \varphi_{2i})/6) * 10^{15}), 256) \tag{15}$$

Step 3: The index sequence index is obtained by arranging the sequence K1 in ascending order. Then, the index sequence is replaced and encrypted with the original image pixels successively to obtain the replaced image P1 as follows

$$P_1(i) = P(\text{index}(K_1(i))) \tag{16}$$

Step 4: The pixels of the sequence K2 and the diagram P1 to be encrypted are different or encrypted as follows

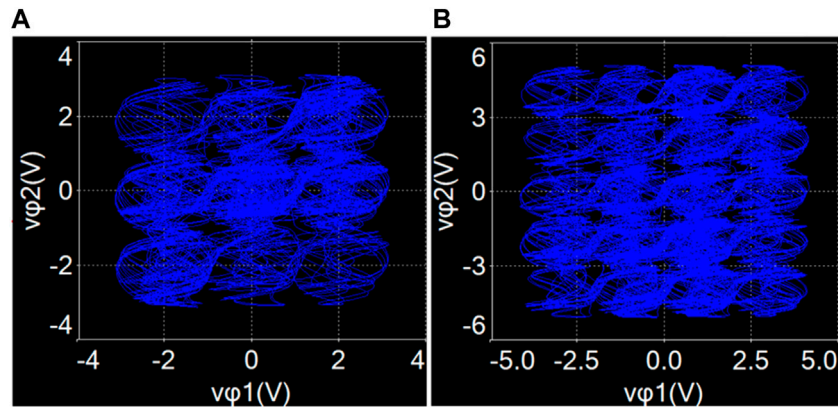


FIGURE 12
Experiment results. (A) 3 × 3-structure attractor. (B) 4 × 5-structure attractor.

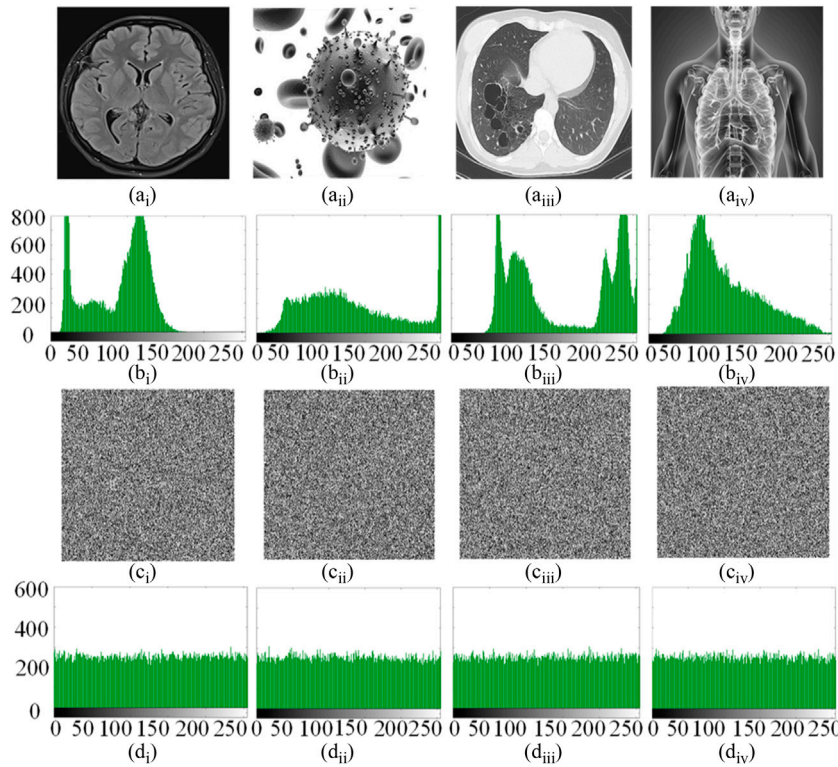


FIGURE 13
Encryption results. (Ai–iv) Original images. (Bi–iv) Histograms of the original images. (Ci–iv) Encrypted images. (Di–iv) Histograms of the encrypted images.

$$C(i) = P_1(i) \oplus K_2(i) \tag{17}$$

brain image, virus image, lung image, and chest image, as shown in Figures 13Ai–Aiv. The key space, histogram, correlation coefficient, information trail, key sensitivity, noise and data loss attacks of the encryption system are analyzed below.

5.2 Encryption performance analysis

In order to prove the effectiveness and security of the above encryption algorithm, the following tests are carried out on the MATLAB R2017a platform. In the experiment, four 256 × 256 medical images were used as original images, which were

- (1) Keyspace analysis. The secret key space is an important index to evaluate the encryption system. Generally speaking, the larger the key space of the encryption system, the stronger the resistance to external brute force attacks. The designed encryption algorithm uses the above 11 parameters as the

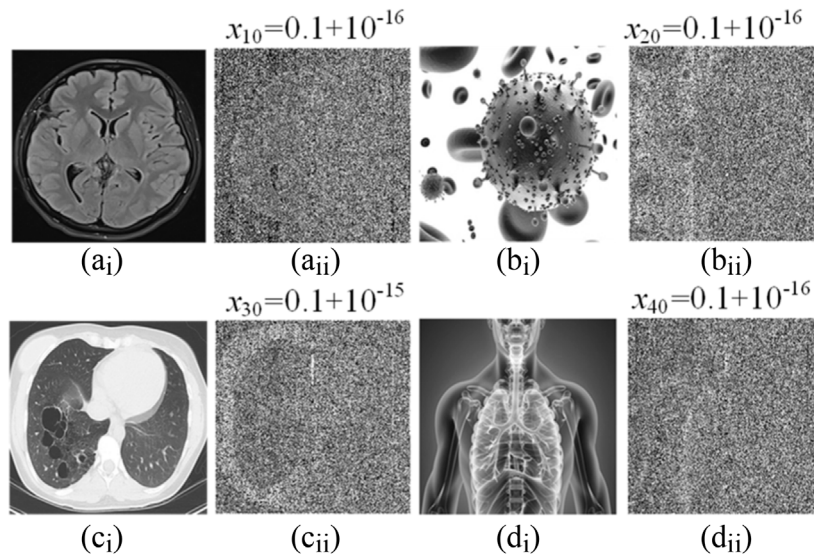


FIGURE 14 Test results of key sensitivity. **(Ai–Di)** Accurate decrypted images with right secret keys. **(Aii–Dii)** Inaccurate decrypted images with wrong secret keys.

secret key, making it difficult to decrypt illegally. In the experiment, all bytes are double-precision data, so the secret key space of the encryption system is $(10^{16})^{11} = 10^{176} \approx 2^{528}$. Obviously, this key space is much larger than the minimum key space value of 2^{100} to resist various brute force attacks.

- (2) Histogram analysis. Histogram is a key index to evaluate the intensity distribution of pixel values in an image. The more average the histogram distribution of the image, the stronger the resistance to statistical attacks. Figure 13 shows the original image, the original image histogram, the encrypted image, and the encrypted image histogram of the four medical images respectively. Figures 13Ci–Civ look confusing and completely lose the information of the original images. In addition, by comparing Figures 14Bi–Biv and Figures 13Di–Div, we can see that the histogram of the encrypted image is very different from that of the original images. The histogram distribution of the original image is completely inconsistent and uneven, while the histogram distribution of the encrypted image is very average. Therefore, the designed encryption algorithm has good security against statistical analysis attacks.
- (3) Correlation analysis. The correlation coefficient is an important index of image robustness. It represents the correlation between two adjacent pixels in an image. Usually, the correlation coefficient of the original image in all directions is relatively large, close to 1. The correlation of the encrypted image should be as small as possible, close to zero. In general, the correlation coefficient of the image can be calculated by the following formula

$$\rho_{xy} = \frac{\sum_{i=1}^N (x_i - E(x))(y_i - E(y))}{\sqrt{\sum_{i=1}^N (x_i - E(x))^2} \sqrt{\sum_{i=1}^N (y_i - E(y))^2}} \quad (18)$$

TABLE 4 Correlation coefficient and information origin between the original image and the encrypted image.

Images		Horizontal	Vertical	Diagonal	Entropy
Brain	Original	0.963966	0.964300	0.936475	6.3463
	Encrypted	0.009911	0.000687	-0.009079	7.9980
Virus	Original	0.965515	0.961770	0.940575	6.0599
	Encrypted	-0.007801	0.003794	0.000667	7.9974
Lung	Original	0.943080	0.954554	0.917790	7.1008
	Encrypted	-0.001244	0.000561	-0.002912	7.9975
Chest	Original	0.960183	0.920840	0.899727	7.4130
	Encrypted	-0.000161	0.001065	-0.002258	7.9975

where x and y represent two adjacent pixel values, and N represents the total number of pixels. $E(x)$ and $E(y)$ represent the average values of pixels x_i and y_i , respectively. In order to calculate the correlation coefficient between the original image and the encrypted image, 10,000 pixels are randomly selected for analysis. Table 4 shows the phase relation values of the four original images and the encrypted images. As can be seen from Table 4, although the correlation coefficients of the four original images are close to 1 in the vertical, horizontal, and diagonal directions, after encryption, the correlation coefficients of the four encrypted images are very close to 0. Therefore, the designed encryption algorithm can greatly reduce the correlation of images, so as to effectively resist statistical attacks.

- (4) Entropy analysis. Information entropy is an important index to describe the degree of image uncertainty. In general, the larger the information origin value, the higher the randomness of the image information. An ideal value for grayscale images is 8. Therefore, a

TABLE 5 Comparison of information entropy of different encryption schemes.

References	[31]	[34]	[35]	[39]	[61]	This work
Entropy	7.9898	7.9976	7.9979	7.9975	7.9976	7.9980

good encryption algorithm should make the information descent of the encryption graph as close to 8 as possible. Information origin can be calculated by the following formula

$$H(P) = \sum_{i=0}^{2^N-1} P(x_i) \log_2 \frac{1}{P(x_i)} \quad (19)$$

where N represents the bit depth of image P , and $P(x_i)$ represents the occurrence probability of pixel x_i . Table 5 shows the information origin values of the four original and encrypted graphs. Obviously, compared with the origin of the original graph, the origin value of the encrypted graph is not only greatly improved, but also very close to the ideal value of 8. Therefore, the encryption algorithm has good encryption performance.

- (5) Sensitivity analysis. The sensitivity of the key is an important index to evaluate the security performance of encryption algorithms. A good encryption algorithm should be as sensitive to the key as possible. When the keys a, b, c, d, ρ, ϕ_0 , and N are fixed and the values of the keys x_{10}, x_{20}, x_{30} , and x_{40} are changed, the key sensitivity of the four images is measured. The experimental results are shown in Figure 15. For the small change of the secret key, even with the disturbance of 10–16, the decrypted image still cannot decrypt the encryption diagram correctly. As shown in Table 6, compared with the existing similar work, the secret key sensitivity value of the image encryption algorithm based on multi-scroll memristor HNN in literature [34] is 10^{-9} , and the secret key sensitivity value of the image encryption algorithm based on multi-scroll chaotic system in literature [35] is 10^{-12} . The designed image encryption algorithm based on multi-structure attractor memristor HNN has great advantages in terms of secret key sensitivity.
- (6) Data loss and noise attacks. Noise and data loss attacks can be used to evaluate the robustness of cryptosystems. On the one hand, the image is prone to sudden and strong noise interference in the transmission process, which will produce noise and affect the correct decryption of the image. Therefore, for image encryption systems, resisting noise attacks is a very important performance index. Here, different proportions of salt and pepper noise are added to the encrypted image, as shown in Figures 15Ai–Aiii. Then the secret key is used to decrypt the encrypted image, as shown in Figures 15Bi–Biii. It can be observed that although some pixels of the decrypted image are changed after the addition of salt and pepper noise, most of the main information of the original image can still be obtained. Therefore, the noise has very little effect on the decryption process of the designed encryption algorithm. On the other hand, it is easy to lose some data in the process of encrypted image transmission. Therefore, a good encryption algorithm should be robust to partial data loss. Here, the data of different sizes of the encryption graph is cut out, as shown in Figures 15Ci–Ciii. Then, using the secret key to decrypt it, the results are shown in Figures 15Di–Diii. Obviously, although the encrypted graph has lost some data information, it can still recover most of the original image information through the decryption process.

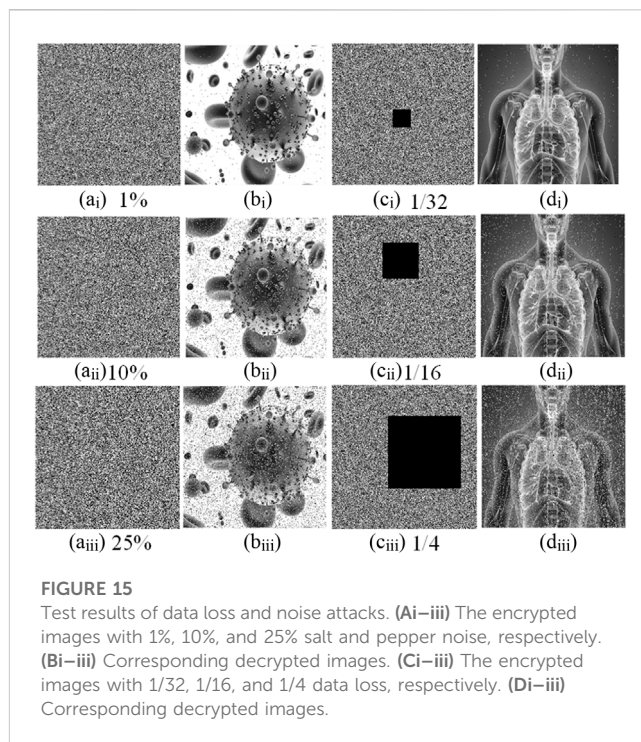


FIGURE 15 Test results of data loss and noise attacks. (Ai–iii) The encrypted images with 1%, 10%, and 25% salt and pepper noise, respectively. (Bi–iii) Corresponding decrypted images. (Ci–iii) The encrypted images with 1/32, 1/16, and 1/4 data loss, respectively. (Di–iii) Corresponding decrypted images.

TABLE 6 Comparison of key sensitivity of different encryption schemes.

References	[32]	[34]	[35]	[39]	[62]	This work
Key sensitivity	10^{-12}	10^{-9}	10^{-12}	10^{-6}	10^{-15}	10^{-16}

TABLE 7 Comparison results of the encryption time.

References	Images	Time (s)
This work	Brain (256 × 256)	0.125
	Virus (512 × 512)	0.273
	Lung (768 × 768)	0.854
[32]	Lena (256 × 256)	0.241
[34]	Lena (256 × 256)	0.876
[35]	Lena (256 × 256)	0.546

- Therefore, the experimental results show that the designed encryption algorithm has strong resistance to data loss attacks.
- (7) Encryption time analysis. Regardless of the security performance, encryption time is also very important, especially in emergency medical care applications. The time test of the scheme is operated using MATLAB R2017a on a PC with Windows 10 64-bit operation system, 2.5 GHz CPU, and 8 GB RAM. All medical images are tested, and the comparison results of one round of encryption execution time are listed in Table 7. It is clear that the execution time of our scheme is shorter than the other schemes.

The above experimental results show that the designed medical image encryption algorithm based on a multi-structure attractor

has a larger key space and higher key sensitivity, can effectively resist various internal and external attacks, and can be applied to protect image data better in practical information communication.

6 Conclusion

Based on the chaotic property of the Hopfield neural network and the memristor synapse control method, a grid multi-structure attractor chaotic system is proposed in this paper. Its complex and varied chaotic structure provides a new idea for the study of new grid chaotic attractors. The basic dynamic analysis, such as equilibrium point, Lyapunov exponential spectrum, power spectrum, bifurcation diagram, and Poincare cross section, shows that the multi-structure chaotic attractor has the characteristics of simple implementation, few control parameters, complex unit topology, expandable unit structure, and complex chaotic dynamics. At the same time, based on the chaotic circuit design method, the circuit simulation of the chaotic attractor is realized, and the feasibility of the system circuit is verified. Finally, combined with the study of chaotic image encryption theory, an image encryption scheme based on the grid multi-structure attractor is designed. The experimental results show that the new grid multi-structure chaotic attractor has certain advantages in encrypted communication and has a good application prospect. The next step will consider introducing multiple memristor synapses into neural networks to construct n -dimensional grid multi-structure chaos attractors to improve the complexity of chaotic systems.

Data availability statement

The original contributions presented in the study are included in the article/Supplementary Material, further inquiries can be directed to the corresponding author.

References

- Pham VT, Volos C, Jafari S, Wei Z, Wang X. Constructing a novel no-equilibrium chaotic system. *Int J Bifurcation Chaos* (2014) 24(05):1450073. doi:10.1142/s0218127414500734
- Lai Q, Kuate PDK, Liu F, Iu HHC. An extremely simple chaotic system with infinitely many coexisting attractors. *IEEE Trans Circuits Syst Express Briefs* (2019) 67(6):1129–33. doi:10.1109/tcsii.2019.2927371
- Wen Z, Wang C, Deng Q, Lin H. Regulating memristive neuronal dynamical properties via excitatory or inhibitory magnetic field coupling. *Nonlinear Dyn* (2022) 110(4):3823–35. doi:10.1007/s11071-022-07813-9
- Lorenz EN. Deterministic nonperiodic flow. *J Atmos Sci* (1963) 20(2):130–41. doi:10.1175/1520-0469(1963)020<0130:dnf>2.0.co;2
- Fan W, Chen X, Wang Y, Chen B, Wu H, Xu Q. Hidden firing patterns and memristor initial condition-offset boosting behavior in a memristive Hindmarsh-Rose neuron model. *Front Phys* (2023) 11:1160419. doi:10.3389/fphy.2023.1160419
- Sun J, Li C, Lu T, Akgul A, Min F. A memristive chaotic system with hypermultistability and its application in image encryption. *Ieee Access* (2020) 8:139289–98. doi:10.1109/access.2020.3012455
- Lin H, Wang C, Du S, Yao W, Sun Y. A family of memristive multibutterfly chaotic systems with multidirectional initial-based offset boosting. *Chaos, Solitons & Fractals* (2023) 172:113518. doi:10.1016/j.chaos.2023.113518
- Sahoo S, Roy BK. A new multi-wing chaotic attractor with unusual variation in the number of wings. *Chaos, Solitons & Fractals* (2022) 164:112598. doi:10.1016/j.chaos.2022.112598
- Chua LO, Lin GN. Canonical realization of Chua's circuit family. *IEEE Trans Circuits Syst* (1990) 37(7):885–902. doi:10.1109/31.55064
- Chen G, Ueta T. Yet another chaotic attractor. *Int J Bifurcation chaos* (1999) 9(07):1465–6. doi:10.1142/s0218127499001024
- Lv J, Chen G. A new chaotic attractor coined. *Int J Bifurcation chaos* (2002) 12(03):659–61.
- Wang Q, Tian Z, Wu X, Tan W. Coexistence of multiple attractors in a novel simple jerk chaotic circuit with CFOAs implementation. *Front Phys* (2022) 10:41. doi:10.3389/fphy.2022.835188
- Njitacke ZT, Sone ME, Fozin TF, Tsafack N, Leutcho GD, Tchagpa CT. Control of multistability with selection of chaotic attractor: Application to image encryption. *Eur Phys J Spec Top* (2021) 230(7-8):1839–54. doi:10.1140/epjs/s11734-021-00137-6
- Yan D, Wang L, Duan S, Chen J, Chen J. Chaotic attractors generated by a memristor-based chaotic system and Julia fractal. *Chaos, Solitons & Fractals* (2021) 146:110773. doi:10.1016/j.chaos.2021.110773
- Liu T, Yan H, Banerjee S, Mou J. A fractional-order chaotic system with hidden attractor and self-excited attractor and its DSP implementation. *Chaos, Solitons & Fractals* (2021) 145:110791. doi:10.1016/j.chaos.2021.110791
- Gong LH, Luo HX, Wu RQ, Zhou NR. New 4D chaotic system with hidden attractors and self-excited attractors and its application in image encryption based on RNG. *Physica A: Stat Mech its Appl* (2022) 591:126793. doi:10.1016/j.physa.2021.126793
- Leonov GA, Kuznetsov NV, Vagaitsev VI. Localization of hidden Chua's attractors. *Phys Lett A* (2011) 375(23):2230–3. doi:10.1016/j.physleta.2011.04.037
- Zhang S, Wang X, Zeng Z. A simple no-equilibrium chaotic system with only one signum function for generating multidirectional variable hidden attractors and its hardware implementation. *Chaos* (2020) 30(5):053129. doi:10.1063/5.0008875

Author contributions

ZH: Methodology, Software, Writing—original draft. HL: Data curation, Formal Analysis, Validation, Investigation, Writing—review and editing. CW: Conceptualization, Funding acquisition, Writing—review and editing.

Funding

The author(s) declare financial support was received for the research, authorship, and/or publication of this article. This work is supported by the National Natural Science Foundation of China (62271197, 61971185, and 62201204), the China Postdoctoral Science Foundation (2022M71104), and the Natural Science Foundation of Hunan Province (2023JJ40168).

Conflict of interest

The authors declare that the research was conducted in the absence of any commercial or financial relationships that could be construed as a potential conflict of interest.

Publisher's note

All claims expressed in this article are solely those of the authors and do not necessarily represent those of their affiliated organizations, or those of the publisher, the editors and the reviewers. Any product that may be evaluated in this article, or claim that may be made by its manufacturer, is not guaranteed or endorsed by the publisher.

19. Chen M, Wang C, Bao H, Ren X, Bao B, Xu Q. Reconstitution for interpreting hidden dynamics with stable equilibrium point. *Chaos, Solitons & Fractals* (2020) 140:110188. doi:10.1016/j.chaos.2020.110188
20. Li C, Peng Y, Tao Z, Sprott JC, Jafari S. Coexisting infinite equilibria and chaos. *Int J Bifurcation Chaos* (2021) 31(05):2130014. doi:10.1142/s0218127421300147
21. Bo-Cheng B, Zhong L, Jian-Ping X. Transient chaos in smooth memristor oscillator. *Chin Phys B* (2010) 19(3):030510. doi:10.1088/1674-1056/19/3/030510
22. Lin H, Wang C, Cui L, Sun Y, Zhang X, Yao W. Hyperchaotic memristive ring neural network and application in medical image encryption. *Nonlinear Dyn* (2022) 110(1):841–55. doi:10.1007/s11071-022-07630-0
23. Wang FP, Wang FQ. Multistability and coexisting transient chaos in a simple memcapacitive system. *Chin Phys B* (2020) 29(5):058502. doi:10.1088/1674-1056/ab7e98
24. Lin H, Wang C, Yu F, Sun J, Du S, Deng Z, et al. A review of chaotic systems based on memristive Hopfield neural networks. *Mathematics* (2023) 11(6):1369. doi:10.3390/math11061369
25. Li S, Wu Y, Zheng G. Adaptive synchronization for hyperchaotic liu system. *Front Phys* (2022) 9:812048. doi:10.3389/fphy.2021.812048
26. Sprott JC. Some simple chaotic flows. *Phys Rev E* (1994) 50(2):647–50. doi:10.1103/physreve.50.r647
27. Sprott JC. A new chaotic jerk circuit. *IEEE Trans Circuits Syst Express Briefs* (2011) 58(4):240–3. doi:10.1109/tcsii.2011.2124490
28. Li C, Yang Y, Yang X, Zi X, Xiao F. A tristable locally active memristor and its application in Hopfield neural network. *Nonlinear Dyn* (2022) 108(2):1697–717. doi:10.1007/s11071-022-07268-y
29. Zhou W, Wang G, Lu HHC, Shen Y, Liang Y. Complex dynamics of a non-volatile memcapacitor-aided hyperchaotic oscillator. *Nonlinear Dyn* (2020) 100:3937–57. doi:10.1007/s11071-020-05722-3
30. Yang Y, Huang L, Xiang J, Guo Q. Three-dimensional sine chaotic system with multistability and multi-scroll attractor. *IEEE Trans Circuits Syst Express Briefs* (2022) 69(3):1792–6. doi:10.1109/tcsii.2021.3126227
31. Wang N, Li C, Bao H, Chen M, Bao B. Generating multi-scroll Chua's attractors via simplified piecewise-linear Chua's diode. *IEEE Trans Circuits Syst Regular Pap* (2019) 66(12):4767–79. doi:10.1109/tcsi.2019.2933365
32. Hong Q, Li Y, Wang X, Zeng Z. A versatile pulse control method to generate arbitrary multidirection multibutterfly chaotic attractors. *IEEE Trans Computer-Aided Des Integrated Circuits Syst* (2018) 38(8):1480–92. doi:10.1109/tcad.2018.2855121
33. Lai Q, Wan Z, Zhang H, Chen G. Design and analysis of multiscroll memristive hopfield neural network with adjustable memductance and application to image encryption. *IEEE Trans Neural Networks Learn Syst* (2022) 1–14. doi:10.1109/tnnls.2022.3146570
34. Lin H, Wang C, Yu F, Xu C, Hong Q, Yao W, et al. An extremely simple multiwing chaotic system: Dynamics analysis, encryption application, and hardware implementation. *IEEE Trans Ind Electron* (2020) 68(12):12708–19. doi:10.1109/tie.2020.3047012
35. Zhang S, Li C, Zheng J, Wang X, Zeng Z, Peng X. Generating any number of initial offset-boosted coexisting Chua's double-scroll attractors via piecewise-nonlinear memristor. *IEEE Trans Ind Electron* (2021) 69(7):7202–12. doi:10.1109/tie.2021.3099231
36. Escalante RJ, Campos E. A class of piecewise linear systems without equilibria with 3-D grid multiscroll chaotic attractors. *IEEE Trans Circuits Syst Express Briefs* (2018) 66(8):1456–60.
37. Ding PF, Feng XY, Wu CM. Novel two-directional grid multi-scroll chaotic attractors based on the Jerk system. *Chin Phys B* (2020) 29(10):108202. doi:10.1088/1674-1056/ab9dea
38. Azam A, Aqeel M, Sunny DA. Generation of multidirectional mirror symmetric multiscroll chaotic attractors (MSMCA) in double wing satellite chaotic system. *Chaos, Solitons & Fractals* (2022) 155:111715. doi:10.1016/j.chaos.2021.111715
39. Peng X, Zeng Y. Image encryption application in a system for compounding self-excited and hidden attractors. *Chaos, Solitons & Fractals* (2020) 139:110044. doi:10.1016/j.chaos.2020.110044
40. Lin H, Wang C, Sun Y. A universal variable extension method for designing multiscroll/wing chaotic systems. *IEEE Trans Ind Electron* (2023) 1–13. doi:10.1109/TIE.2023.3299020
41. Xu C, Wang C, Jiang J, Sun J, Lin H. Memristive circuit implementation of context-dependent emotional learning network and its application in multitask. *IEEE Trans Computer-Aided Des Integrated Circuits Syst* (2021) 41(9):3052–65. doi:10.1109/tcad.2021.3116463
42. Liao M, Wang C, Sun Y, Lin H, Xu C. Memristor-based affective associative memory neural network circuit with emotional gradual processes. *Neural Comput Appl* (2022) 34(16):13667–82. doi:10.1007/s00521-022-07170-z
43. Jiang D, Njitacke ZT, Nkapkop JDD, Tsafack N, Wang X, Awrejcewicz J. A new cross ring neural network: Dynamic investigations and application to WBAN. *IEEE Internet Things J* (2022) 10(8):7143–52. doi:10.1109/jiot.2022.3228748
44. Zhou C, Wang C, Yao W, Lin H. Observer-based synchronization of memristive neural networks under DoS attacks and actuator saturation and its application to image encryption. *Appl Maths Comput* (2022) 425:127080. doi:10.1016/j.amc.2022.127080
45. Zhou C, Wang C, Sun Y, Yao W, Lin H. Cluster output synchronization for memristive neural networks. *Inf Sci* (2022) 589:459–77. doi:10.1016/j.ins.2021.12.084
46. Hopfield JJ. Neurons with graded response have collective computational properties like those of two-state neurons. *Proc Natl Acad Sci* (1984) 81(10):3088–92. doi:10.1073/pnas.81.10.3088
47. Bao B, Chen C, Bao H, Zhang X, Xu Q, Chen M. Dynamical effects of neuron activation gradient on Hopfield neural network: Numerical analyses and hardware experiments. *Int J Bifurcation Chaos* (2019) 29(04):1930010. doi:10.1142/s0218127419300106
48. Lin H, Wang C, Chen C, Sun Y, Zhou C, Xu C, et al. Neural bursting and synchronization emulated by neural networks and circuits. *IEEE Trans Circuits Syst Regular Pap* (2021) 68(8):3397–410. doi:10.1109/tcsi.2021.3081150
49. Isaac SD, Njitacke ZT, Tsafack N, Tchappa CT, Kengne J. Novel compressive sensing image encryption using the dynamics of an adjustable gradient Hopfield neural network. *Eur Phys J Spec Top* (2022) 231(10):1995–2016. doi:10.1140/epjs/s11734-022-00472-2
50. Chen C, Min F, Zhang Y, Bao H. ReLU-type Hopfield neural network with analog hardware implementation. *Chaos, Solitons & Fractals* (2023) 167:113068. doi:10.1016/j.chaos.2022.113068
51. Lin H, Wang C, Sun Y, Tang Z, Xie F, Chen D, et al. Analysis of outer membrane vesicles indicates that glycerophospholipid metabolism contributes to early symbiosis between *Sinorhizobium fredii* HH103 and soybean. *IEEE Trans Circuits Syst Express Briefs* (2022) 70(1):311–22. doi:10.1094/MPMI-11-21-0288-R
52. Yu F, Kong X, Mokbel AAM, Yao W, Cai S. Complex dynamics, hardware implementation and image encryption application of multiscroll memristive Hopfield neural network with a novel local active memristor. *IEEE Trans Circuits Syst Express Briefs* (2022) 70(1):326–30. doi:10.1109/tcsii.2022.3218468
53. Yu F, Shen H, Yu Q, Kong X, Sharma PK, Cai S. Privacy protection of medical data based on multi-scroll memristive Hopfield neural network. *IEEE Trans Netw Sci Eng* (2022) 10(2):845–58. doi:10.1109/tNSE.2022.3223930
54. Lai Q, Wan Z, Kuate PDK. Generating grid multi-scroll attractors in memristive neural networks. *IEEE Trans Circuits Syst Regular Pap* (2022) 70(3):1324–36. doi:10.1109/tcsi.2022.3228566
55. Strukov DB, Snider GS, Stewart DR, Williams RS. The missing memristor found. *nature* (2008) 453(7191):80–3. doi:10.1038/nature06932
56. Xia Z, Wang C, Jin J, Du S, Lin H, Yang H. Novel AM/FM/ASK/FSK/PSK/QAM signal generator based on a digitally programmable CDTA. *Circuits, Systems, Signal Process*. (2015) 34(5):1635–53. doi:10.1007/s00034-014-9921-3
57. Liu X, Wang J. The simplest memristor circuit with hyperchaos. *Front Phys* (2022) 10:904200. doi:10.3389/fphy.2022.904200
58. Wang M, An M, He S, Zhang X, Ho-Ching Iu H, Li Z. Two-dimensional memristive hyperchaotic maps with different coupling frames and its hardware implementation. *Chaos* (2023) 33(7):073129. doi:10.1063/5.0154516
59. He S, Liu J, Wang H, Sun K. A discrete memristive neural network and its application for character recognition. *Neurocomputing* (2023) 523:1–8. doi:10.1016/j.neucom.2022.12.014
60. Zhu W, Sun K, He S, Wang H, Liu W. A class of m-dimension grid multi-cavity hyperchaotic maps and its application. *Chaos, Solitons & Fractals* (2023) 170:113370. doi:10.1016/j.chaos.2023.113370
61. Sambas A, Vaidyanathan S, Zhang X, Koyuncu I, Bonny T, Tuna M, et al. A novel 3D chaotic system with line equilibrium: Multistability, integral sliding mode control, electronic circuit, FPGA implementation and its image encryption. *IEEE Access* (2022) 10:68057–74. doi:10.1109/access.2022.3181424
62. Sambas A, Vaidyanathan S, Tlelo-Cuautle E, Abd-El-Atty B, El-Latif AAA, Guillen-Fernandez O, et al. A 3-D multi-stable system with a peanut-shaped equilibrium curve: Circuit design, FPGA realization, and an application to image encryption. *IEEE Access* (2020) 8:137116–32. doi:10.1109/access.2020.3011724